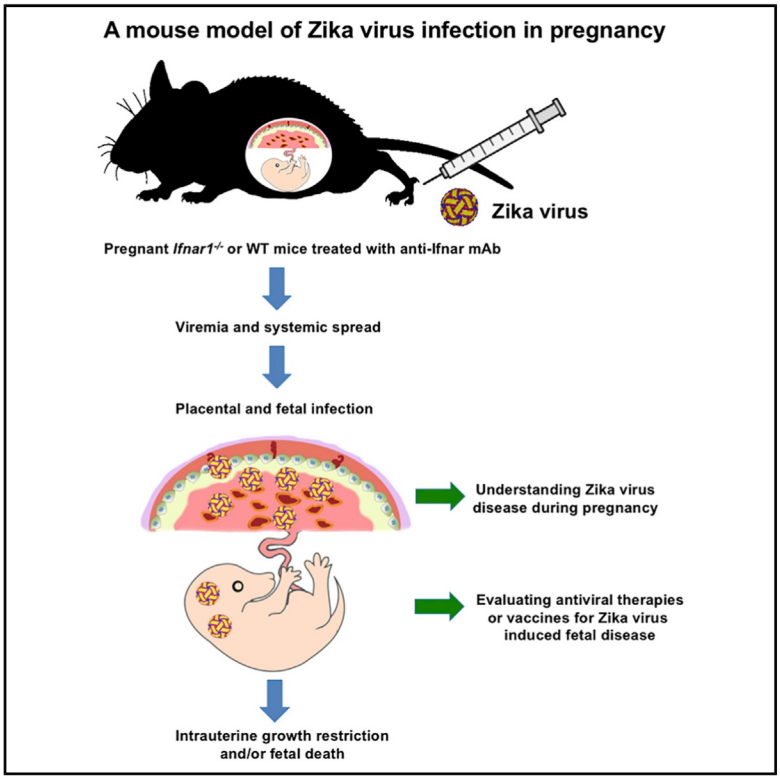
Article

Cell

Zika Virus Infection during Pregnancy in Mice Causes Placental Damage and Fetal Demise

Graphical Abstract



Highlights

- Establishment of an in utero transmission model of ZIKV infection
- ZIKV infects placental cells and results in intrauterine growth restriction
- ZIKV infection and injury of the fetal brain is observed
- ZIKV infection of fetuses can occur by a trans-placental route

Authors

Jonathan J. Miner, Bin Cao, Jennifer Govero, ..., Kevin K. Noguchi, Indira U. Mysorekar, Michael S. Diamond

Correspondence

mysorekari@wudosis.wustl.edu (I.U.M.), diamond@borcim.wustl.edu (M.S.D.)

In Brief

Zika virus infection of mice early in pregnancy results in infection of the placenta and fetal brain, causing a fetal syndrome that resembles the intrauterine growth restriction and spontaneous abortion observed in ZIKV-infected pregnant women.

Miner et al., 2016, Cell *165*, 1081–1091
May 19, 2016 © 2016 Elsevier Inc.
http://dx.doi.org/10.1016/j.cell.2016.05.008

Takeda Vaccines EX2031
IPR2025-00776
U.S. Patent No. 11,730,802

Cell

Zika Virus Infection during Pregnancy in Mice Causes Placental Damage and Fetal Demise

Jonathan J. Miner,[1,8] Bin Cao,[5,8] Jennifer Govero,[1,8] Amber M. Smith,[1] Estefania Fernandez,[1,4] Omar H. Cabrera,[6] Charise Garber,[1] Michelle Noll,[1] Robyn S. Klein,[1,2,3,4] Kevin K. Noguchi,[6] Indira U. Mysorekar,[4,5,*] and Michael S. Diamond[1,3,4,7,*]

[1]Department of Medicine
[2]Department of Anatomy and Neurobiology
[3]Department of Molecular Microbiology
[4]Department of Pathology and Immunology
[5]Department of Obstetrics and Gynecology
[6]Department of Psychiatry
[7]The Center for Human Immunology and Immunotherapy Programs
Washington University School of Medicine, Saint Louis, MO 63110, USA
[8]Co-first authors
*Correspondence: mysorekari@wudosis.wustl.edu (I.U.M.), diamond@borcim.wustl.edu (M.S.D.)
http://dx.doi.org/10.1016/j.cell.2016.05.008

SUMMARY

Zika virus (ZIKV) infection in pregnant women causes intrauterine growth restriction, spontaneous abortion, and microcephaly. Here, we describe two mouse models of placental and fetal disease associated with in utero transmission of ZIKV. Female mice lacking type I interferon signaling (*Ifnar1*$^{-/-}$) crossed to wild-type (WT) males produced heterozygous fetuses resembling the immune status of human fetuses. Maternal inoculation at embryonic day 6.5 (E6.5) or E7.5 resulted in fetal demise that was associated with ZIKV infection of the placenta and fetal brain. We identified ZIKV within trophoblasts of the maternal and fetal placenta, consistent with a trans-placental infection route. Antibody blockade of Ifnar1 signaling in WT pregnant mice enhanced ZIKV trans-placental infection although it did not result in fetal death. These models will facilitate the study of ZIKV pathogenesis, in utero transmission, and testing of therapies and vaccines to prevent congenital malformations.

INTRODUCTION

Zika virus (ZIKV) is a mosquito-transmitted flavivirus that was first isolated from a febrile rhesus macaque in Uganda in 1947 and is related to other globally relevant arthropod-transmitted human pathogens including dengue (DENV), yellow fever (YFV), West Nile (WNV), Japanese encephalitis (JEV), and tick-borne encephalitis viruses (Lazear and Diamond, 2016). Over the last decade, ZIKV has emerged from a relatively obscure status to causing large epidemics in Micronesia, French Polynesia, and South and Central America. Although in most instances ZIKV infection results in a self-limiting febrile illness associated with rash and conjunctivitis, severe neurological phenotypes can occur, including Guillain-Barre syndrome and meningoencephalitis (Carteaux et al., 2016; Oehler et al., 2014). Infection in pregnant women is of major concern, as it is linked to catastrophic fetal abnormalities including microcephaly, spontaneous abortion, and intrauterine growth restriction (IUGR) due to placental insufficiency (Brasil et al., 2016). Because of the growing public health concern, there is an urgent need to establish animal models of intrauterine ZIKV infection that define mechanisms of fetal transmission and facilitate testing of therapeutics and vaccines. Furthermore, an in utero animal model of ZIKV infection would establish causality and satisfy the criteria for proof of teratogenicity (Rasmussen et al., 2016).

In 2015, Brazil experienced a sharp rise in the number of cases of pregnancy-associated microcephaly, and this was linked to a concurrent epidemic of ZIKV infection. Mounting evidence suggests that ZIKV infection in pregnant women causes congenital abnormalities and fetal demise (Brasil et al., 2016; Sarno et al., 2016; Ventura et al., 2016). Initial case descriptions of microcephaly and spontaneous abortion have been bolstered by evidence of viral RNA and antigen in the brains of congenitally infected fetuses and newborns (Martines et al., 2016; Mlakar et al., 2016). These findings were substantiated by a prospective study of a cohort of symptomatic, ZIKV-infected pregnant women in which 29% of fetuses exhibited developmental abnormalities including microcephaly and IUGR, which in a subset of cases resulted in fetal demise or stillbirth (Brasil et al., 2016). Preliminary reports suggest that ZIKV-induced fetal abnormalities can occur in all trimesters of pregnancy although the most severe manifestations are associated with infections in the first and second trimesters (Brasil et al., 2016). Congenital abnormalities associated with ZIKV infection also have been described in French Polynesia (by retrospective analysis) and other Latin American countries (Cauchemez et al., 2016). These findings suggest that ZIKV strains in French Polynesia and Latin America share the potential to cause disease during pregnancy.

Recently, we and others have developed models of ZIKV pathogenesis in adult mice that recapitulated several features of human disease (Aliota et al., 2016; Lazear et al., 2016; Rossi et al.,

2016). Whereas 4- to 6-week-old wild-type (WT) mice did not develop overt clinical illness after infection with a contemporary clinical strain of ZIKV, mice lacking the ability to produce or respond to type I interferon (IFN) (e.g., *Ifnar1*$^{-/-}$ mice) developed severe neurological disease that was associated with high viral loads in the brain and spinal cord and substantial lethality. In a complementary approach using WT mice treated with a blocking anti-ifnar antibody (MAR1-5A3), we reported a less severe model of ZIKV pathogenesis that also resulted in replication of ZIKV in several organs (Lazear et al., 2016). These animals, however, survived infection and did not develop neurological signs or neuroinvasive disease.

Given the urgent need to understand the basis for in utero transmission of ZIKV and its pathological consequences, we developed two models of ZIKV infection during pregnancy using *Ifnar1*$^{-/-}$ females crossed to WT males as well as pregnant WT females treated with an anti-ifnar-blocking antibody. We found that ZIKV infects pregnant dams and the placenta, and this resulted in damage to the placental barrier and infection of the developing fetus, as well as placental insufficiency and IUGR. In severe cases, ZIKV infection of *Ifnar1*$^{-/-}$ females led to fetal demise. When dams were treated with an anti-ifnar antibody, infection of the developing fetus occurred but was less severe and did not cause fetal death. These findings establish models for studying mechanisms of in utero transmission and testing of candidate therapies for preventing congenital malformations. They also highlight the concern that ZIKV infection can occur in fetuses of otherwise healthy-appearing dams with uncertain neurodevelopmental consequences.

RESULTS

Since the type I interferon (IFN) response prevents efficient replication of ZIKV in peripheral organs of WT mice (Lazear et al., 2016), we initially used *Ifnar1*$^{-/-}$ mice to facilitate high levels of ZIKV replication during pregnancy. *Ifnar1*$^{-/-}$ female mice were bred with WT males so that resulting fetuses would be heterozygous (*Ifnar1*$^{+/-}$) and thus exhibit a largely intact type I IFN signaling response. In parallel, we developed a second model of ZIKV infection during pregnancy by treating WT pregnant dams with an anti-ifnar-blocking antibody 1 day prior to infection (Figure 1A). Both sets of pregnant mice were inoculated via a subcutaneous route in the footpad with 10^3 focus forming units (FFU) of a clinical isolate from French Polynesia (H/PF/2013) that was passaged in Vero cells. This ZIKV strain is at least 97% identical at the nucleotide level to the sequence of an epidemic strain of ZIKV in Brazil (Calvet et al., 2016; Faria et al., 2016). We confirmed the sequence of our ZIKV H/PF/2013 stock by next-generation sequencing (data not shown), which also allowed us to exclude the presence of adventitious pathogens.

In the *Ifnar1*$^{-/-}$ model, pregnant dams mated with WT mice were inoculated on embryonic days 6.5 (E6.5) and E7.5 and sacrificed on E13.5 and E15.5, respectively (Figure 1A). To minimize confounding effects of maternal illness on fetal viability, we evaluated pregnant *Ifnar1*$^{-/-}$ mice prior to the onset of disease, which is characterized by hunched posture, fur ruffling, or hindlimb paralysis (Lazear et al., 2016). Individual fetuses were evaluated morphologically for size and appearance by measuring the crown-rump length and the occipito-frontal diameter of the fetal head, the latter of which establishes microcephaly in human fetuses (Chervenak et al., 1987; Staples et al., 2016). By E13.5, the majority of ZIKV-infected *Ifnar1*$^{+/-}$ heterozygous fetuses had undergone fetal demise and been resorbed, leaving only a placental remnant (Figures 1B, upper, and 1C). The remaining intact *Ifnar1*$^{+/-}$ fetuses exhibited significant IUGR (60.2 mm^2 versus 48.7 mm^2, $p < 0.0001$, Figure 1D). In ZIKV-infected pregnant women, multiple phenotypes have been described including fetal demise, IUGR, and microcephaly (Brasil et al., 2016; Sarno et al., 2016). Although we did not observe isolated microcephaly in this in utero model of ZIKV infection, several other abnormalities were visible in ZIKV-infected *Ifnar1*$^{+/-}$ fetuses, including pallor and foci of necrotic tissue in the placenta (Figure 1B).

To determine whether direct infection of the placenta and fetus occurred, we measured ZIKV RNA levels by quantitative real-time RT-PCR (qRT-PCR) as well as infectious virus by plaque assay. High levels of viral RNA and infectious virus were detected within the placenta and also within the fetus head by E13.5 (Figures 1E and 1F and Figures S1A and S1B). As seen with the fetuses from dams infected on E6.5, ZIKV inoculation on E7.5 also resulted in fetal demise and resorption by E15.5 as well as growth restriction (141.8 mm^2 versus 79.5 mm^2, $p < 0.0001$, Figure 1H) and pallor (Figure 1B) of intact fetuses. As expected from prior studies with *Ifnar1*$^{-/-}$ males (Lazear et al., 2016; Rossi et al., 2016), high levels of ZIKV were present in the blood, spleen, and brain of *Ifnar1*$^{-/-}$ dams at day 7 after infection (Figures 1I–1K). Of note, the amount of ZIKV RNA within the placenta was ~1,000-fold greater than in maternal serum (Figures 1F and 1I), suggesting that ZIKV replicates preferentially within this tissue.

In our second model of ZIKV infection during pregnancy, WT mice were treated with MAR1-5A3, a blocking anti-ifnar monoclonal antibody (Sheehan et al., 2006), on E5.5, inoculated with ZIKV on E6.5 or E7.5, and fetuses were analyzed on E13.5 or E15.5, respectively (Figure 1A). Although demise was not observed, fetuses exhibited evidence of IUGR compared to control mAb-treated and mock-infected animals (62.3 mm^2 versus 50.2 mm^2, $p < 0.005$), albeit to a lesser extent than seen in *Ifnar1*$^{+/-}$ animals (Figure 1D). In contrast, anti-ifnar mAb-treated mice inoculated subcutaneously with 10^3 FFU of a clinical DENV serotype 3 (DENV-3) isolate that replicates in mice (Pinto et al., 2015; Sarathy et al., 2015) did not exhibit evidence of placental or fetal infection by qRT-PCR or signs of IUGR (Figure 1D and data not shown). These results suggest that ZIKV may have greater tropism for placental cells than other flaviviruses.

The levels of ZIKV RNA detected in WT fetuses were affected by the dose of anti-ifnar mAb administered, with the greatest amounts of ZIKV RNA present in fetuses receiving 2 or 3 mgs of anti-ifnar mAb (Figure 1E). ZIKV RNA persisted in the anti-ifnar mAb-treated fetal heads and bodies at least through E16.5 (Figures S1C and S1D), a critical time in early development of the mouse brain. The placentas in both the *Ifnar1*$^{-/-}$ and anti-ifnar antibody models exhibited higher levels of infection than the fetal tissues, and ZIKV RNA accumulation in the placenta was

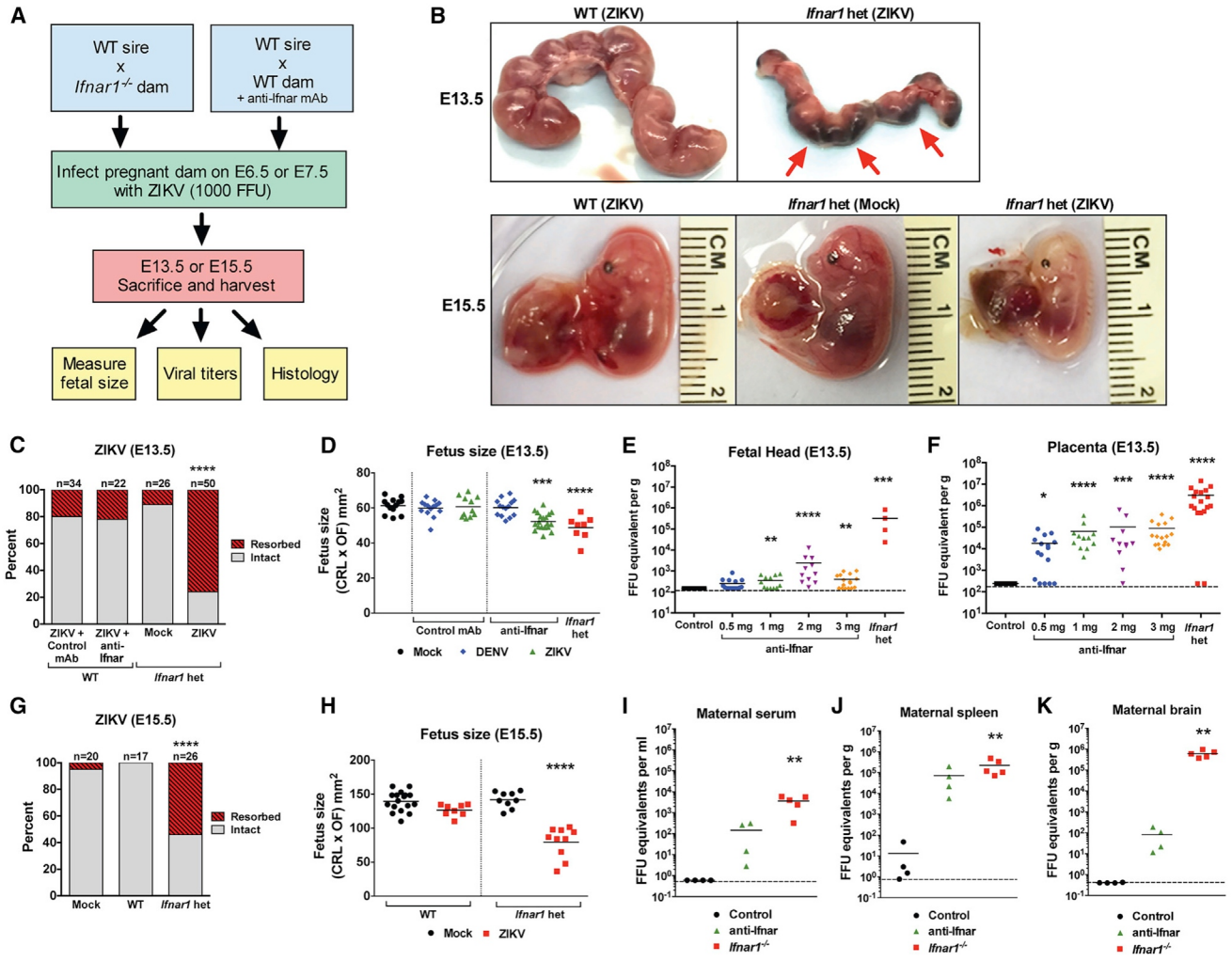


Figure 1. Mortality, Viral Burden, and Size of Mouse Fetuses after Maternal Infection with ZIKV

(A) Schematic depiction of two models of infection during pregnancy. Model 1: WT males were crossed with *Ifnar1*$^{-/-}$ dams. Pregnant dams were infected subcutaneously with ZIKV (10^3 FFU) on E6.5 or E7.5 followed by harvest on E13.5, or 15.5, respectively. Model 2: WT males were crossed with WT dams. Pregnant dams treated with 1 mg of an anti-ifnar antibody on days −1, +1, and +3 relative to ZIKV (10^3 FFU) or DENV-3 (10^3 FFU) infection. Mice were sacrificed on E13.5 or E15.5 and fetuses and placentas were harvested for measurements of fetal size by crown-rump length (CRL) and occipito-frontal (OF) diameter.

(B) E13.5 uteri from ZIKV-infected WT and *Ifnar1*$^{-/-}$ dams. Most *Ifnar1*$^{+/-}$ fetuses carried by *Ifnar1*$^{-/-}$ dams died in utero and had undergone resorption, leaving only the residual placenta. In the lower three panels are representative images of fetuses carried by ZIKV-infected WT and mock-infected *Ifnar1*$^{-/-}$ dams, the latter of which exhibited growth restriction at E15.5.

(C) Fetus survival on E13.5 after infection with ZIKV on E6.5. Mice were either treated with three 1 mg doses of control or anti-ifnar antibody (left two bars) or untreated mock- or ZIKV-infected *Ifnar1*$^{-/-}$ dams (right two bars). Data are representative of at least 3 independent experiments with 1 pregnant female dam per experiment. The n for each group is indicated above each bar. ****$p < 0.0001$.

(D) Fetus size as assessed by CRL x OF diameter in E13.5 fetuses following E6.5 infection of the indicated pregnant dams with either ZIKV or DENV-3. For these experiments, a total dose of 3 mg of anti-ifnar antibody was used. Bars indicate the mean size of 8-20 fetuses from 2 or 3 independent experiments from fetuses carried by 2 to 3 pregnant dams. ***$p < 0.0005$; ****$p < 0.0001$.

(E and F) Viral burden was measured by qRT-PCR assay from the fetal head and placenta on E13.5 after infection at E6.5. Symbols represent individual fetuses pooled from several independent experiments with the exception of 4 intact *Ifnar1*$^{+/-}$ fetal heads that were carried by a single dam. Bars indicate the mean of 4 to 17 mice per group. Dotted lines represent the limit of sensitivity of the assay. *$p < 0.05$ **$p < 0.005$; ***$p < 0.0005$; ****$p < 0.0001$.

(G) Fetus survival on E15.5 after infection with ZIKV on E7.5. Data are representative of at least 2 independent experiments with 1 pregnant female dam per experiment. The n for each group is indicated above each bar. ****$p < 0.0001$.

(H) Fetus size as assessed by CRL x OF diameter in E15.5 fetuses following E7.5 infection of the indicated pregnant dams with ZIKV. ****$p < 0.0001$.

(I–K) Viral burden was measured by qRT-PCR assay from maternal serum, spleen, and brain at E13.5. Symbols are derived from individual animals and pooled from 2 or 3 independent experiments. Bars indicate the mean of 4 to 5 mice per group. Dotted lines represent the limit of sensitivity of the assay. See also Figure S1.

independent of the anti-ifnar mAb dose above 0.5 mg (Figure 1F). In comparison, mice treated with the isotype control antibody sustained low levels or no detectable ZIKV infection in the placenta, fetal heads or maternal tissues (Figure 1E, 1F, and 1I–1K). Collectively, these data suggest that the mouse placenta is vulnerable to infection with ZIKV, and that high-grade infection may cause placental insufficiency, IUGR, and fetal demise, at least in *Ifnar1*$^{+/-}$ animals. Anti-ifnar mAb-treated animals sustained less infection and no enhanced lethality although a mild IUGR phenotype was observed.

We evaluated ZIKV localization in the placenta to define whether transmission occurred by a trans-placental route. The mouse placenta is comprised of the maternal decidua and the fetal embryo-derived compartments, including the junctional and labyrinth zones (Figure 2A). Different types of trophoblasts with distinct functions reside within all three layers, including trophoblast giant cells, glycogen trophoblasts, and spongiotrophoblasts. Within the labyrinth zone, fetal capillaries are lined by fetal blood vessel endothelium, which are separated from maternal sinusoids by a layer of mononuclear trophoblasts and a syncytiotrophoblast bilayer (Figure 2A) (Simmons and Cross, 2005; Watson and Cross, 2005). We performed RNA fluorescence in situ hybridization (FISH) coupled with histopathological analysis in ZIKV-infected *Ifnar1*$^{+/-}$ placentas and confirmed the presence of ZIKV RNA in different trophoblast cells, including glycogen trophoblasts and spongiotrophoblasts (Figure 2B) and to a lesser extent in mononuclear trophoblasts and syncytiotrophoblasts (data not shown). These findings are consistent with cell culture studies demonstrating ZIKV infection of human trophoblast cell lines (Bayer et al., 2016) and suggest that the mouse model of infection during pregnancy recapitulates features of human disease including placental tropism of ZIKV. We independently confirmed ZIKV infection and replication in two of three human trophoblast cell lines (Figure S2). Transmission electron microscopy of placentas revealed multiple 50 nm dense bodies within the endoplasmic reticulum of the mononuclear trophoblasts (Figure 2C, left), consistent with ZIKV infection of the maternal placenta. As these bodies resemble flavivirus virions (Allison et al., 2003) and were not present in uninfected animals, they are suggestive for the presence of virus. Proximity to non-nucleated maternal erythrocytes (Figure 2C, left) confirmed the location as within the maternal face of the placenta. Consistent with a trans-placental route of infection, we also observed bodies resembling virions within the endoplasmic reticulum of fetal endothelial cells that lined damaged fetal capillaries (Figure 2C, right). The cellular and ultrastructural evidence of ZIKV infection in trophoblasts and fetal endothelium suggests that maternal viremia leads to compromise of the placental barrier by infecting fetal trophoblasts and entering the fetal circulation.

Pathological analysis of ZIKV-infected *Ifnar1*$^{-/-}$ (maternal) and *Ifnar1*$^{+/-}$ (fetal) placentas showed severe vascular injury characterized by irregularly shaped, reduced fetal capillaries and destruction of the placental microvasculature (Figures 3A and 3B, Ifnar het severe). Infected *Ifnar1*$^{-/-}$ placentas were smaller, mostly because the labyrinth zone was markedly thinned. In addition, apoptotic trophoblasts were evident in ZIKV-infected placentas (Figure 3A, black arrows). Immunofluorescence staining of pan-cytokeratin, a pan-trophoblast marker, was diminished in infected *Ifnar1*$^{-/-}$ placentas, consistent with evidence of apoptotic trophoblasts (Figure 3B). Apoptosis in trophoblasts can cause disruption of the placental barrier, which compromises protection against pathogens (Robbins and Bakardjiev, 2012). Indeed, ZIKV-infected *Ifnar1*$^{+/-}$ placentas contained large numbers of nucleated fetal erythrocytes (Figure 3A, blue arrows), key indicators of fetal stress. Evidence of vascular damage and fewer blood vessels also was reflected by diminished staining of vimentin, a marker of fetal blood vessels in mouse placentas (Figure 3B).

Histopathological assessment of ZIKV-infected *Ifnar1*$^{+/-}$ fetal brains demonstrated abundant apoptotic cells within multiple regions at E13.5 (Figures 4A–4D). Activated caspase-3 staining showed low levels of physiological apoptosis in uninfected fetuses (Figures 4E–4H), whereas infected animals had apoptotic cells throughout the midbrain and hindbrain (Figures 4B–4D and 4I). Although we could localize viral RNA in infected placentas, multiple attempts at RNA FISH staining of ZIKV-infected fetal brains did not yield a clear pattern of viral RNA expression (data not shown), despite the recovery of infectious virus (Figures S1A and S1B). Accordingly, we cannot state with certainty whether the enhanced apoptosis within ZIKV-infected fetuses results from infection-induced apoptosis or another process, including ischemia due to placental insufficiency. The presence of numerous apoptotic cells within the developing central nervous system (CNS) coupled with the established neurotropism of ZIKV (Lazear et al., 2016), however, suggests direct infection may contribute.

DISCUSSION

Epidemiological studies have found that ZIKV infection during pregnancy causes catastrophic neurodevelopmental outcomes in human fetuses, but there currently is no effective treatment or prevention of ZIKV infection other than avoidance of its mosquito vectors. Given the devastating effects of this rapidly emerging infectious disease, small animal models of ZIKV infection during pregnancy are urgently needed to test candidate therapeutics and vaccines that could prevent or mitigate intrauterine infection with ZIKV. We developed two mouse models that support ZIKV replication and trans-placental transmission in pregnant dams: (1) a model of severe disease in pregnant *Ifnar1*$^{-/-}$ dams that resulted in fetal demise; and (2) a less severe model of ZIKV pathogenesis in utero using pregnant WT dams that were given anti-ifnar antibody prior to and during infection, which resulted in mild IUGR and viral infection within the fetal head during a key period in neurodevelopment.

The placenta acts as a barrier against infections, due to multiple unique structural, cellular, and immune properties. The detrimental effects of congenital viruses on pregnancy and fetal outcomes occur in part because of impaired trophoblast function (Arechavaleta-Velasco et al., 2002). Defective placentas can lead to severe maternal and fetal morbidity and mortality during pregnancy, including spontaneous abortion, stillbirth, preterm birth, IUGR, and other complications. We observed profound pathological changes in ZIKV-infected placentas, including

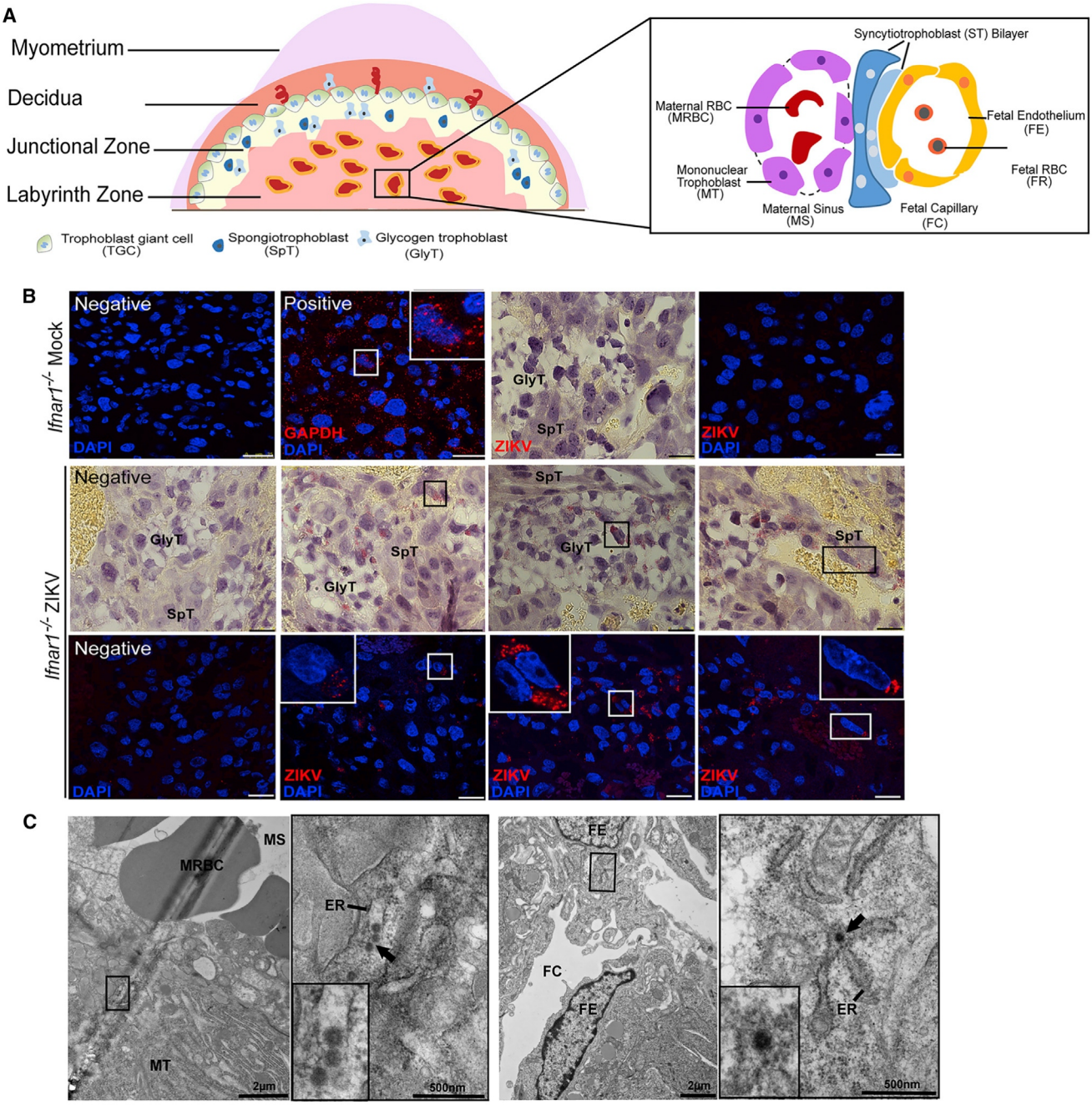


Figure 2. ZIKV Infects Trophoblasts and Endothelial Cells within Mouse Placentas

Pregnant *Ifnar1*$^{-/-}$ dams were infected on E7.5 with 10^3 FFU of ZIKV via a subcutaneous route and placentas were harvested on E15.5 for histological analysis.

(A) Schematic representation of the mouse placental structure.

(B) Representative RNA FISH images in uninfected and infected *Ifnar1*$^{-/-}$ placentas. Images in each column correspond to the same field of view generated under bright-field or confocal microscopy. Higher magnification of images is displayed as inserts. Scale bar, 25 μm.

(C) Transmission electron microscopy images of ZIKV infected *Ifnar1*$^{-/-}$ placentas. ZIKV particles were identified within the endoplasmic reticulum in the maternal sinus (left), and in the fetal endothelium (right) lining fetal capillaries in the labyrinth layer.

MT = Mononuclear trophoblast; MS = Maternal sinus; FE = Fetal endothelial cell; FC = Fetal capillary; MRBC = Maternal erythrocyte; and ER = Endoplasmic reticulum. See also Figure S2.

trophoblast apoptosis, abnormal fetal capillary features, and increased fetal nucleated erythrocytes, indicating malfunction of mouse placentas caused by ZIKV infection.

We observed variability in susceptibility to ZIKV infection of different human trophoblast cell lines. Trophoblast cell lines (JEG-3 and HTR-8) originally cultured from choriocarcinoma

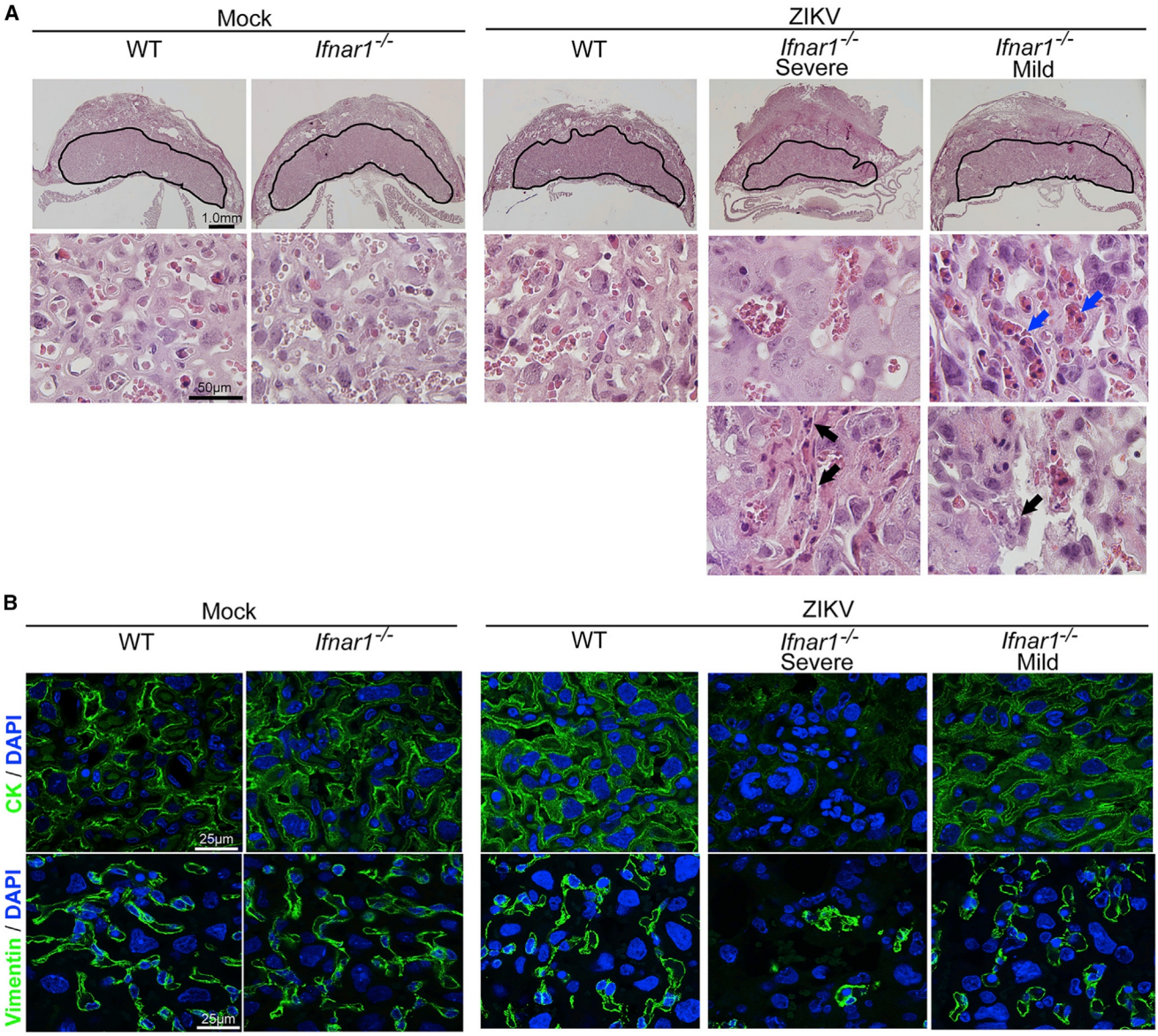


Figure 3. ZIKV Infection Triggers Apoptosis and Vascular Damage in the Placenta

Pregnant dams were infected on E7.5 with 10^3 FFU of ZIKV via a subcutaneous route and placentas were harvested on E15.5 for histological analysis.

(A) Representative hematoxylin and eosin staining showed pathological features of placentas at E15.5. Labyrinth layers were marked with a solid line on the cross section of mouse placentas. Black arrows indicate apoptotic trophoblasts. Blue arrows indicate increased number of nucleated fetal erythrocytes in fetal capillaries.

(B) Immunofluorescence staining of cytokeratin (CK) and vimentin in mouse placentas. CK, a marker for trophoblasts; vimentin, a marker for the endothelium in fetal capillaries.

See also Figure S2.

explants and first trimester human villous explants, respectively, which exhibit features of extravillous trophoblasts (EVTs) including high invasive capacity and expression of HLA-G, a MHC class II molecule, were susceptible to ZIKV infection. In contrast, a relatively undifferentiated cytotrophoblast cell line (BeWo) was not. Previous studies have shown that EVTs are most susceptible to bacterial infections, particularly during the first and second trimesters (Cao and Mysorekar, 2014; Robbins and Bakardjiev, 2012; Zeldovich and Bakardjiev, 2012). Thus, it is possible that in early pregnancy, ZIKV infects EVTs and enters the fetal circulation. Placentas nearer to term, which have reduced EVTs on the tips of anchoring villi and a more fully developed placental barrier, in general exhibit greater resistance to infection. Indeed, human primary trophoblasts of the villous syncytiotrophoblast phenotype from term placentas were resistant to ZIKV

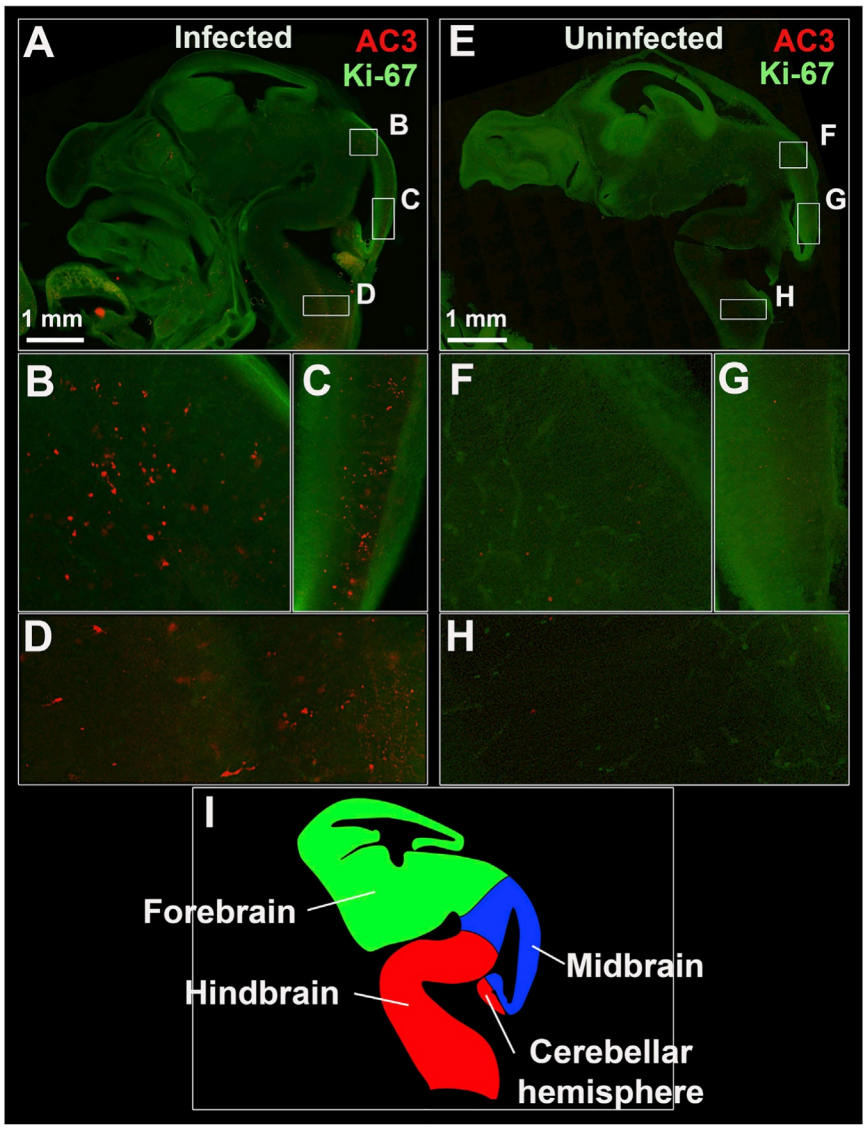


Figure 4. ZIKV Infection Is Associated with Evidence of Apoptosis in the Fetal Brain

Pregnant *Ifnar1*$^{-/-}$ dams were infected with 10^3 FFU of ZIKV via a subcutaneous route. Infected (left) or uninfected (right) *Ifnar1*$^{+/-}$ E13.5 fetuses were stained with the apoptotic marker activated caspase-3 (AC3; red) and the proliferative marker Ki-67 (green).

(A and E) Sagittal images of representative infected (A) and uninfected (E) fetal heads showing high expression of Ki-67 along brain regions adjacent to ventricles indicative of proliferating neural progenitor cells in the neuroepithelium.

(B-H) Lettered box regions (B-D and F-H) in these images are magnified in corresponding panels below. Higher levels of apoptosis can be seen in the midbrain (B-C) and hindbrain (D) of the infected *Ifnar1*$^{+/-}$ fetus. Alternatively, low levels of physiological apoptosis are seen in the absence of infection (F-H).

(I) Diagram depicting the developing E13.5 fetal brain in sagittal view including the forebrain (green), midbrain (blue), and hindbrain (red).

Images are representative of 4-5 sections per fetus from 2 fetuses.

infection due to the production of IFN-λ in paracrine manner (Bayer et al., 2016).

Several aspects of our models of ZIKV infection during pregnancy resemble intrauterine infection by ZIKV in humans. Common features included tropism of ZIKV for the placenta, evidence of intrauterine infection, and fetal demise. However, infection during pregnancy in mice did not recapitulate all aspects of human disease, as we did not detect microcephaly, brain calcifications, or absence of individual brain structures, such as the corpus callosum. There are several reasons why ZIKV may not have induced these pathological manifestations in our models. In mice, brain neurogenesis begins around E10 (Finlay and Darlington, 1995), and the brain of a newborn pup is relatively immature at postnatal day 1, akin to the developmental stage of the human brain at mid-gestation (Semple et al., 2013). As the development of the mouse brain includes a major postnatal component, examination of the neurodevelopmental effects of ZIKV infection in mice may require infection later during pregnancy. Since ZIKV infects mature neurons as well as neural cell progenitors and limits their growth (Tang et al., 2016), the morphological effects of ZIKV infection on brain development may be more apparent in species with larger cerebral cortices.

Although ZIKV-associated microcephaly has drawn major public health and media attention, ZIKV infection of human fetuses does not always cause this manifestation, and the sequelae of intrauterine infection in the absence of gross morphological abnormalities remain to be defined. In pregnant WT dams that were treated with an anti-ifnar antibody, we observed only mild growth restriction in the developing fetus although ZIKV RNA was detectable in the fetal head at both E13.5 and E16.5 after infection. Future behavioral studies may define whether intrauterine infection by ZIKV has long-term neurological effects in mice and serves as a model for evaluation of disease in humans (Staples et al., 2016).

We found that the murine placentas can be infected by ZIKV. Infection of *Ifnar1*$^{-/-}$ dams led to severe placental damage and destruction of the microvasculature, which most likely limited blood flow to the developing fetus and caused severe IUGR, ischemia, and fetal demise. In vivo infection of the mouse placenta with ZIKV may provide a model for defining host factors required for or that restrict infection, which could suggest a path for developing therapies to limit placental and intrauterine infection. For example, since IFN-λ restricts ZIKV replication within human trophoblasts from term placentas

(Bayer et al., 2016), studies are planned to test the effects of exogenously administered IFN-λ on in utero transmission in mice.

Maternal-fetal transmission of pathogens can be mediated by diverse pathways, with the most common being via an ascending route and hemochorial transmission. Viruses from the urogenital tract can disseminate into intrauterine space and colonize the fetal membrane or the placenta in an ascending manner (Edwards et al., 2015). In contrast, viruses from the maternal blood circulation can be transported to the feto-maternal space and infect trophoblasts lining the maternal-fetal interface. These trophoblasts include the EVTs, which embed in maternal decidua, endovascular extravillous cytotrophoblasts, and villous trophoblasts, which are bathed in maternal blood (Delorme-Axford et al., 2014). Our studies suggest that ZIKV can infect the placenta through blood-placental transmission and bypass the placental barrier to infect the fetus. Nonetheless, ascending infection routes might be important in sexual transmission during pregnancy. ZIKV has been found in human semen (Musso et al., 2015) and mouse testes (Lazear et al., 2016; Rossi et al., 2016) and can be transmitted sexually from male to female in humans (Musso et al., 2015).

Intrauterine infection with flaviviruses may be an underappreciated phenomenon. Prior to the ZIKV epidemic, there were isolated descriptions of trans-placental infection in humans with other flaviviruses including WNV and JEV (Chaturvedi et al., 1980; Nguyen et al., 2002). These reports suggest that sporadic cases of flavivirus-induced miscarriage or fetal demise might have been unrecognized, although this remains speculative. We are currently testing whether additional variations in ZIKV infection (e.g., dose, route of administration, virus strain, time of infection during pregnancy, and time of analysis) in our mouse model of in utero transmission can recapitulate other morphological abnormalities in the CNS that are described in human disease. Of note, intrauterine infection with Saint Louis encephalitis virus, a less well studied flavivirus, caused severe neurological outcomes in mice. In that model, disease depended on the gestational date of infection (Andersen and Hanson, 1970); mice infected early in gestation survived, whereas those inoculated later developed neurological malformations and died as neonates (Andersen and Hanson, 1970; Andersen and Hanson, 1975). In our studies with DENV and an anti-ifnar-blocking antibody, inoculation of mice did not result in placental infection, although it is possible that this was due to a diminished ability of DENV to replicate in mice compared to ZIKV. Experiments that test infection of pregnant animals with additional related viruses may clarify whether placental infection is an underappreciated clinical manifestation of flavivirus pathogenesis.

Treatment and prevention of ZIKV infection will likely require small animal models for testing of vaccines and potential therapies. The mouse models described in our study may be relevant to studying mechanisms of pathogenesis and determining whether vaccines given prior to pregnancy can prevent infection in the developing fetus. Mouse models of ZIKV infection during pregnancy also may provide fundamental insights into how the placental barrier prevents viral infection from the developing fetus, and why this process fails in the context of specific pathogens. Finally, our animal model of in utero transmission establishes causality of a fetal syndrome associated with ZIKV infection in mice.

EXPERIMENTAL PROCEDURES

Ethics Statement

This study was carried out in accordance with the recommendations in the Guide for the Care and Use of Laboratory Animals of the National Institutes of Health. The protocols were approved by the Institutional Animal Care and Use Committee at the Washington University School of Medicine (Assurance number A3381-01). Inoculations were performed under anesthesia induced and maintained with ketamine hydrochloride and xylazine, and all efforts were made to minimize animal suffering.

Viruses and Titration

Vero cells (African green monkey kidney epithelial cells) were maintained in DMEM supplemented with 5% fetal bovine serum (Omega) and L-glutamine at 37°C with 5% CO_2. ZIKV strain H/PF/2013 (French Polynesia, 2013) was provided by the Arbovirus Branch of the Centers for Disease Control and Prevention with permission (X. de Lamballerie, Aix Marseille Université) (Baronti et al., 2014). ZIKV stocks were propagated in Vero cells and titrated by focus-forming assay (FFA). Infected cell foci were detected at 48 hr after infection, following fixation with 1% paraformaldehyde and incubation with 500 ng/mL of flavivirus cross-reactive mouse monoclonal antibody E60 (Oliphant et al., 2006) for 2 hr at room temperature. After incubation for 1 hr with a 1:5,000 dilution of horseradish peroxidase (HRP)-conjugated goat anti-mouse IgG (Sigma), foci were detected by addition of TrueBlue substrate (KPL). Foci were analyzed with a CTL Immunospot instrument. Studies with ZIKV were conducted under biosafety level 2 (BSL2) and animal BSL3 (A-BSL3) containment.

Mouse Experiments

Ifnar1$^{-/-}$ mice (Hwang et al., 1995) were backcrossed onto a C57BL/6 background. Mice were bred in a specific-pathogen-free facility at Washington University, or purchased (WT animals) from Jackson Laboratories. Mice were set up for timed-matings and at embryonic days E6.5 or E7.5 were inoculated with ZIKV by subcutaneous (footpad) route with 10^3 FFU of ZIKV in 50 μL of PBS. Mice were sacrificed at E13.5, E15.5, or E16.5 depending on the experimental design. Placentas and fetuses were harvested from the infected mice. Fetus size was measured as the crown-rump length × occipito-frontal diameter of the head. In some experiments, WT mice were treated with indicated doses of an Ifnar-blocking mouse mAb (MAR1-5A3) or isotype control mouse mAb (GIR-208) (produced by Leinco Technologies) (Sheehan et al., 2006; Sheehan et al., 2015) by intraperitoneal injection prior to and after ZIKV or DENV-3 infection.

Measurement of Viral Burden

ZIKV-infected pregnant mice were euthanized on E13.5, E15.5, or E16.5. Placentas and fetal heads were weighed and homogenized with zirconia beads in a MagNA Lyser instrument (Roche Life Science) in 250 or 500 μL of PBS. All homogenized tissues from infected animals were stored at −80°C until virus titration. With some samples, viral burden was determined by plaque assay on Vero cells. Samples were thawed, clarified by centrifugation (2,000 × *g* at 4°C for 10 min), and then diluted serially prior to infection of Vero cells. Plaque assays were overlaid with low-melt agarose, and 4 days later were fixed with 10% formaldehyde and stained with crystal violet (Brien et al., 2013). Tissue samples and serum from ZIKV-infected mice were extracted with the RNeasy Mini Kit (tissues) or Viral RNA Mini Kit (serum) (QIAGEN). ZIKV RNA levels were determined by one-step quantitative reverse transcriptase PCR (qRT-PCR) on an ABI 7500 Fast Instrument using standard cycling conditions. Viral burden was expressed on a $\log_{10}$ scale as viral RNA equivalents per g or per mL after comparison with a standard curve produced using serial 10-fold dilutions of ZIKV RNA. A published primer set was used to detect ZIKV RNA (Lanciotti et al., 2008): Fwd, 5′-CCGCTGCCCAACACAAG-3′; Rev, 5′-CCACTAACGTTC TTTTGCAGACAT-3′; Probe, 5′-/56-FAM/AGCCTACCT/ZEN/TGACAAGCAAT CAGACACTCAA/3IABkFQ/-3′, (Integrated DNA Technologies).

RNA Fluorescence *In Situ* Hybridization

RNA FISH was performed using ViewRNA ISH Tissue 2-Plex Assay kit (Affymetrix) according to the manufacturer's instructions. Formalin-fixed paraffin-embedded tissue sections were hydrated, heat-treated for 10 min at 90°C, and digested with protease for 20 min. Endogenous alkaline phosphatase was inactivated with 0.2 M HCl and 300 mM NaCl at room temperature for 15 min before the probe hybridization. The probe targeting ZIKV RNA was designed and synthesized by Affymetrix and was based on the ZIKV French Polynesian 2013 genomic RNA sequence (accession number SAMN04592777). Positive controls (probe-targeting housekeeping genes) and no-probe negative controls were included in all samples. Tissues were counterstained with DAPI and Gill's hematoxylin and visualized using standard bright-field and confocal microscopes.

Immunohistochemistry and Immunofluorescence Imaging

Fetuses were removed by Caesarian-section on E13.5, post-fixed in 4% paraformaldehyde, and sectioned at 70 μM with a vibratome. Immunohistochemistry was performed by immersing sections in blocking solution and incubating overnight in primary antibodies raised against activated caspase-3 (AC3; Cell Signaling) and Ki-67 (BD-Biosciences). Subsequently, sections were rinsed and reacted with fluorescent secondary antibodies.

Harvested placentas were fixed in 10% neutral buffered formalin (Fisher) at room temperature and embedded in paraffin. At least three placentas from different litters with the indicated treatments were sectioned and stained with hematoxylin and eosin to assess morphology. For immunofluorescence staining of mouse placentas, deparaffinized tissues were blocked in buffer (1% BSA, 0.3% Triton, 1 × PBS) for 2 hr and incubated with primary antibodies overnight. The following primary antibodies were used: cytokeratin (1:500, rabbit, DAKO Z0622) and vimentin (1:500, rabbit, Abcam ab92547). After rinsing with PBS, secondary antibody conjugated with Alexa 488 (1:500 in PBS) was applied for 1 hr at room temperature. Samples were counterstained with DAPI (4'6'-diamidino-2-phenilindole, 1:1,000 dilution) for 10 min and mounted in Prolong Gold (Life Technologies). RNA FISH imaging of mouse placentas was acquired using a TSC SPE inverted confocal microscope (Leica) using a 63× objective. Histology images were captured by use of a Nikon Eclipse microscope equipped with an Olympus DP71 color camera under 20× and 40× objectives.

Transmission Electron Microscopy

Mouse placental samples were fixed in 2% paraformaldehyde and 2.5% glutaraldehyde (Polysciences) in 100 mM sodium cacodylate buffer for 1 hr at room temperature and overnight at 4°C, washed in cacodylate buffer, post-fixed in 1% osmium tetroxide (Polysciences) for 1 hr, then rinsed with distilled H_2O before en bloc staining with 1% aqueous uranyl acetate (Ted Pella) for 1 hr. Samples were dehydrated in a graded series of ethanol and embedded in Eponate 12 resin (Ted Pella). Sections (90 nm thick) were cut with a Leica Ultracut UCT ultramicrotome, stained with uranyl acetate and lead citrate, and imaged on a JEOL 1200 EX transmission electron microscope (JEOL USA).

mAb Generation

A more complete description of the anti-ZIKV mAbs will be provided in a forthcoming manuscript (E. Fernandez, D. Platt, and M. Diamond, unpublished data). Briefly, to create ZV-2, *Irf3*$^{-/-}$ mice were infected and boosted with 10^3 FFU of ZIKV (MR-766 and H/PF/2013, respectively) and given a final intravenous boost with live 10^6 FFU of ZIKV (H/F/2013) 3 days prior to fusion with P3X63 myeloma cells. Hybridomas secreting antibodies that reacted with ZIKV-infected Vero cells were identified by flow cytometry and cloned by limiting dilution. ZV-2 was purified by protein A affinity chromatography.

Cell Culture and Infection

JEG-3 and BeWo cells were obtained from ATCC and cultured in F12/DMEM media supplemented with 10% FBS (Life Technologies) at 37°C with 5% CO_2. HTR-8/SVneo cells were provided by C. H. Graham (Queen's University) and maintained in RPMI 1640 media with 5% FBS. For flow cytometry and viral yield assays, trophoblast cell lines were seeded in 24-well plates at 5 × 10^5 cells per well. For immunofluorescence staining, trophoblast cell lines were cultured in 4-well chamber slides (Millipore). Cells were counted and infected with ZIKV at a MOI 0.1 for 2 hr, washed twice with warm PBS and cultured with fresh medium. At indicated time points after infection, supernatants were harvested for virus titration, and cells were trypsinized for flow cytometry or fixed for immunofluorescence staining using ZV-2, a ZIKV-specific mAb.

Data Analysis

All data were analyzed with GraphPad Prism software. For viral burden analysis, the log titers and levels of viral RNA were analyzed by the Mann-Whitney test or ANOVA. A p value of < 0.05 indicated statistically significant differences. Significance of the survival rates were assessed by Chi-square test. The morphological measurements were assessed by a Mann-Whitney test or by a 2-way ANOVA.

SUPPLEMENTAL INFORMATION

Supplemental Information includes two figures and can be found with this article online at http://dx.doi.org/10.1016/j.cell.2016.05.008.

AUTHOR CONTRIBUTIONS

J.J.M., J.G., B.C., K.K.N., R.S.K., I.U.M., and M.S.D. designed experiments. J.J.M., B.C., J.G, A.M.S, O.H.C., E.F., C.G., M.N., and K.K.N. performed the experiments. J.J.M, B.C, I.U.M., and M.S.D. analyzed the data. J.J.M., B.C., I.U.M., and M.S.D. wrote the first draft of the paper; all authors edited the manuscript.

ACKNOWLEDGMENTS

This work was supported by grants from the NIH (R01 AI073755 and R01 AI104972 to M.S.D., R01 HD052664 to K.K.N., and R01 NS052632 to R.S.K.) and the Intellectual and Developmental Disabilities Research Center at Washington University (NIH/NICHD U54 HD087011). J.J.M., E.F., and D.J.P. were supported by a Rheumatology Research Foundation Scientist Development Award, NIH Pre-doctoral training grant award (T32 AI007163), and the NIH Research Education Program (R25 HG006687), respectively. The work also was supported by a Preventing Prematurity Initiative grant from the Burroughs Wellcome Fund and a Prematurity Research Initiative Investigator award from the March of Dimes (to I.U.M). We thank Wandy Betty for her TEM assistance, Fredrik Kraus for his expertise in placental pathology, and Justin Richner for advice with establishing the RNA FISH assays. Finally, we acknowledge Xavier de Lamballerie (Emergence des Pathologies Virales, Aix-Marseille Université, Marseille, France) and the European Virus Archive goes Global (EVAg) for consenting to the use of H/PF/2013 ZIKV strain for this study under a material transfer agreement with the EVAg parter, Aix-Marseille Université. M.S.D. is a consultant for Inbios, Visterra, and Takeda Pharmaceuticals and on the Scientific Advisory Boards of Moderna and OraGene.

Received: April 24, 2016
Revised: May 2, 2016
Accepted: May 2, 2016
Published: May 11, 2016

REFERENCES

Aliota, M.T., Caine, E.A., Walker, E.C., Larkin, K.E., Camacho, E., and Osorio, J.E. (2016). Characterization of Lethal Zika Virus Infection in AG129 Mice. PLoS Negl. Trop. Dis. *10*, e0004682.

Allison, S.L., Tao, Y.J., O'Riordain, G., Mandl, C.W., Harrison, S.C., and Heinz, F.X. (2003). Two distinct size classes of immature and mature subviral particles from tick-borne encephalitis virus. J. Virol. *77*, 11357–11366.

Andersen, A.A., and Hanson, R.P. (1970). Experimental transplacental transmission of st. Louis encephalitis virus in mice. Infect. Immun. *2*, 320–325.

Andersen, A.A., and Hanson, R.P. (1975). Intrauterine infection of mice with St. Louis encephalitis virus: immunological, physiological, neurological, and behavioral effects on progeny. Infect. Immun. *12*, 1173–1183.

Arechavaleta-Velasco, F., Koi, H., Strauss, J.F., 3rd, and Parry, S. (2002). Viral infection of the trophoblast: time to take a serious look at its role in abnormal implantation and placentation? J. Reprod. Immunol. *55*, 113–121.

Baronti, C., Piorkowski, G., Charrel, R.N., Boubis, L., Leparc-Goffart, I., and de Lamballerie, X. (2014). Complete coding sequence of zika virus from a French polynesia outbreak in 2013. Genome Announc. *2*, e00500–e00514.

Bayer, A., Lennemann, N.J., Ouyang, Y., Bramley, J.C., Morosky, S., Marques, E.T., Jr., Cherry, S., Sadovsky, Y., and Coyne, C.B. (2016). Type III Interferons Produced by Human Placental Trophoblasts Confer Protection against Zika Virus Infection. Cell Host Microbe *16*, 30100–30107.

Brasil, P., Pereira, J.P., Jr., Raja Gabaglia, C., Damasceno, L., Wakimoto, M., Ribeiro Nogueira, R.M., Carvalho de Sequeira, P., Machado Siqueira, A., Abreu de Carvalho, L.M., Cotrim da Cunha, D., et al. (2016). Zika Virus Infection in Pregnant Women in Rio de Janeiro - Preliminary Report. N. Engl. J. Med. Published online March 4, 2016. http://dx.doi.org/10.1056/NEJMoa1602412.

Brien, J.D., Lazear, H.M., and Diamond, M.S. (2013). Propagation, quantification, detection, and storage of west nile virus. Current protocols in microbiology *31*, 15D 13 11–15D 13 18.

Calvet, G., Aguiar, R.S., Melo, A.S.O., Sampaio, S.A., de Filippis, I., Fabri, A., Araujo, E.S.M., de Sequeira, P.C., de Mendonça, M.C.L., de Oliveira, L., et al. (2016). Detection and sequencing of Zika virus from amniotic fluid of fetuses with microcephaly in Brazil: a case study. Lancet Infect. Dis. S1473-3099(16)00095-5.

Cao, B., and Mysorekar, I.U. (2014). Intracellular bacteria in placental basal plate localize to extravillous trophoblasts. Placenta *35*, 139–142.

Carteaux, G., Maquart, M., Bedet, A., Contou, D., Brugières, P., Fourati, S., Cleret de Langavant, L., de Broucker, T., Brun-Buisson, C., Leparc-Goffart, I., and Mekontso Dessap, A. (2016). Zika Virus Associated with Meningoencephalitis. N. Engl. J. Med. *374*, 1595–1596.

Cauchemez, S., Besnard, M., Bompard, P., Dub, T., Guillemette-Artur, P., Eyrolle-Guignot, D., Salje, H., Van Kerkhove, M.D., Abadie, V., Garel, C., et al. (2016). Association between Zika virus and microcephaly in French Polynesia, 2013–15: a retrospective study. The Lancet, *epub ahead of print*.

Chaturvedi, U.C., Mathur, A., Chandra, A., Das, S.K., Tandon, H.O., and Singh, U.K. (1980). Transplacental infection with Japanese encephalitis virus. J. Infect. Dis. *141*, 712–715.

Chervenak, F.A., Rosenberg, J., Brightman, R.C., Chitkara, U., and Jeanty, P. (1987). A prospective study of the accuracy of ultrasound in predicting fetal microcephaly. Obstet. Gynecol. *69*, 908–910.

Delorme-Axford, E., Sadovsky, Y., and Coyne, C.B. (2014). The Placenta as a Barrier to Viral Infections. Annu Rev Virol *1*, 133–146.

Edwards, M.S., Popek, E.J., Wise, B., Hatzenbuehler, L., Arunachalam, A.R., and Hair, A.B. (2015). Ascending in utero herpes simplex virus infection in an initially healthy-appearing premature infant. Pediatr. Dev. Pathol. *18*, 155–158.

Faria, N.R., Azevedo, Rdo.S., Kraemer, M.U.G., Souza, R., Cunha, M.S., Hill, S.C., Thézé, J., Bonsall, M.B., Bowden, T.A., Rissanen, I., et al. (2016). Zika virus in the Americas: Early epidemiological and genetic findings. Science *352*, 345–349.

Finlay, B.L., and Darlington, R.B. (1995). Linked regularities in the development and evolution of mammalian brains. Science *268*, 1578–1584.

Hwang, S.Y., Hertzog, P.J., Holland, K.A., Sumarsono, S.H., Tymms, M.J., Hamilton, J.A., Whitty, G., Bertoncello, I., and Kola, I. (1995). A null mutation in the gene encoding a type I interferon receptor component eliminates antiproliferative and antiviral responses to interferons alpha and beta and alters macrophage responses. Proc. Natl. Acad. Sci. USA *92*, 11284–11288.

Lanciotti, R.S., Kosoy, O.L., Laven, J.J., Velez, J.O., Lambert, A.J., Johnson, A.J., Stanfield, S.M., and Duffy, M.R. (2008). Genetic and serologic properties of Zika virus associated with an epidemic, Yap State, Micronesia, 2007. Emerg. Infect. Dis. *14*, 1232–1239.

Lazear, H.M., and Diamond, M.S. (2016). Zika Virus: New Clinical Syndromes and Its Emergence in the Western Hemisphere. J. Virol. *90*, 4864–4875.

Lazear, H.M., Govero, J., Smith, A.M., Platt, D.J., Fernandez, E., Miner, J.J., and Diamond, M.S. (2016). A Mouse Model of Zika Virus Pathogenesis. Cell Host Microbe, S1931-3128(16)30102-0.

Martines, R.B., Bhatnagar, J., Keating, M.K., Silva-Flannery, L., Muehlenbachs, A., Gary, J., Goldsmith, C., Hale, G., Ritter, J., Rollin, D., et al. (2016). Notes from the Field: Evidence of Zika Virus Infection in Brain and Placental Tissues from Two Congenitally Infected Newborns and Two Fetal Losses - Brazil, 2015. MMWR Morb. Mortal. wkly. Rep. *65*, 159–160.

Mlakar, J., Korva, M., Tul, N., Popović, M., Poljšak-Prijatelj, M., Mraz, J., Kolenc, M., Resman Rus, K., Vesnaver Vipotnik, T., Fabjan Vodušek, V., et al. (2016). Zika Virus Associated with Microcephaly. N. Engl. J. Med. *374*, 951–958.

Musso, D., Roche, C., Robin, E., Nhan, T., Teissier, A., and Cao-Lormeau, V.M. (2015). Potential sexual transmission of Zika virus. Emerg. Infect. Dis. *21*, 359–361.

Nguyen, Q., Morrow, C., Novick, L., Cambareri, C., Olson, B., Aubry, R., Snedeker, J., Anand, M., Huang, C., Morse, D., et al.; Centers for Disease Control and Prevention (CDC) (2002). Intrauterine West Nile virus infection–New York, 2002. MMWR Morb. Mortal. wkly. Rep. *51*, 1135–1136.

Oehler, E., Watrin, L., Larre, P., Leparc-Goffart, I., Lastère, S., Valour, F., Baudouin, L., Mallet, H., Musso, D., and Ghawche, F. (2014). Zika virus infection complicated by Guillain-Barre syndrome–case report, French Polynesia, December 2013. Euro Surveill. *19*, 20720.

Oliphant, T., Nybakken, G.E., Engle, M., Xu, Q., Nelson, C.A., Sukupolvi-Petty, S., Marri, A., Lachmi, B.-E., Olshevsky, U., Fremont, D.H., et al. (2006). Antibody recognition and neutralization determinants on domains I and II of West Nile Virus envelope protein. J. Virol. *80*, 12149–12159.

Pinto, A.K., Brien, J.D., Lam, C.-Y.K., Johnson, S., Chiang, C., Hiscott, J., Sarathy, V.V., Barrett, A.D., Shresta, S., and Diamond, M.S. (2015). Defining New Therapeutics Using a More Immunocompetent Mouse Model of Antibody-Enhanced Dengue Virus Infection. MBio *6*, e01316–e15.

Rasmussen, S.A., Jamieson, D.J., Honein, M.A., and Petersen, L.R. (2016). Zika Virus and Birth Defects - Reviewing the Evidence for Causality. N. Engl. J. Med. Published online April 13, 2016. http://dx.doi.org/10.1056/NEJMsr1604338.

Robbins, J.R., and Bakardjiev, A.I. (2012). Pathogens and the placental fortress. Curr. Opin. Microbiol. *15*, 36–43.

Rossi, S.L., Tesh, R.B., Azar, S.R., Muruato, A.E., Hanley, K.A., Auguste, A.J., Langsjoen, R.M., Paessler, S., Vasilakis, N., and Weaver, S.C. (2016). Characterization of a Novel Murine Model to Study Zika Virus. Am. J. Trop. Med. Hyg. 16-0111.

Sarathy, V.V., White, M., Li, L., Gorder, S.R., Pyles, R.B., Campbell, G.A., Milligan, G.N., Bourne, N., and Barrett, A.D.T. (2015). A lethal murine infection model for dengue virus 3 in AG129 mice deficient in type I and II interferon receptors leads to systemic disease. J. Virol. *89*, 1254–1266.

Sarno, M., Sacramento, G.A., Khouri, R., do Rosário, M.S., Costa, F., Archanjo, G., Santos, L.A., Nery, N., Jr., Vasilakis, N., Ko, A.I., and de Almeida, A.R. (2016). Zika Virus Infection and Stillbirths: A Case of Hydrops Fetalis, Hydranencephaly and Fetal Demise. PLoS Negl. Trop. Dis. *10*, e0004517.

Semple, B.D., Blomgren, K., Gimlin, K., Ferriero, D.M., and Noble-Haeusslein, L.J. (2013). Brain development in rodents and humans: Identifying benchmarks of maturation and vulnerability to injury across species. Prog. Neurobiol. *106-107*, 1–16.

Sheehan, K.C., Lai, K.S., Dunn, G.P., Bruce, A.T., Diamond, M.S., Heutel, J.D., Dungo-Arthur, C., Carrero, J.A., White, J.M., Hertzog, P.J., et al. (2006). Blocking monoclonal antibodies specific for mouse IFN-alpha/beta receptor subunit 1 (IFNAR-1) from mice immunized by in vivo hydrodynamic transfection. Journal of interferon & cytokine research *26*, 804–819.

Sheehan, K.C., Lazear, H.M., Diamond, M.S., and Schreiber, R.D. (2015). Selective Blockade of Interferon-α and -β Reveals Their Non-Redundant Functions in a Mouse Model of West Nile Virus Infection. PLoS ONE *10*, e0128636.

Simmons, D.G., and Cross, J.C. (2005). Determinants of trophoblast lineage and cell subtype specification in the mouse placenta. Dev. Biol. *284*, 12–24.

Staples, J.E., Dziuban, E.J., Fischer, M., Cragan, J.D., Rasmussen, S.A., Cannon, M.J., Frey, M.T., Renquist, C.M., Lanciotti, R.S., Muñoz, J.L., et al. (2016). Interim Guidelines for the Evaluation and Testing of Infants with Possible Congenital Zika Virus Infection - United States, 2016. MMWR Morb. Mortal. wkly. Rep. *65*, 63–67.

Tang, H., Hammack, C., Ogden, S.C., Wen, Z., Qian, X., Li, Y., Yao, B., Shin, J., Zhang, F., Lee, E.M., et al. (2016). Zika Virus Infects Human Cortical Neural Progenitors and Attenuates Their Growth. Cell Stem Cell. Published online March 4, 2016. http://dx.doi.org/10.1016/j.stem.2016.02.016.

Ventura, C.V., Maia, M., Bravo-Filho, V., Góis, A.L., and Belfort, R., Jr. (2016). Zika virus in Brazil and macular atrophy in a child with microcephaly. Lancet *387*, 228.

Watson, E.D., and Cross, J.C. (2005). Development of structures and transport functions in the mouse placenta. Physiology (Bethesda) *20*, 180–193.

Zeldovich, V.B., and Bakardjiev, A.I. (2012). Host defense and tolerance: unique challenges in the placenta. PLoS Pathog. *8*, e1002804.

Cell

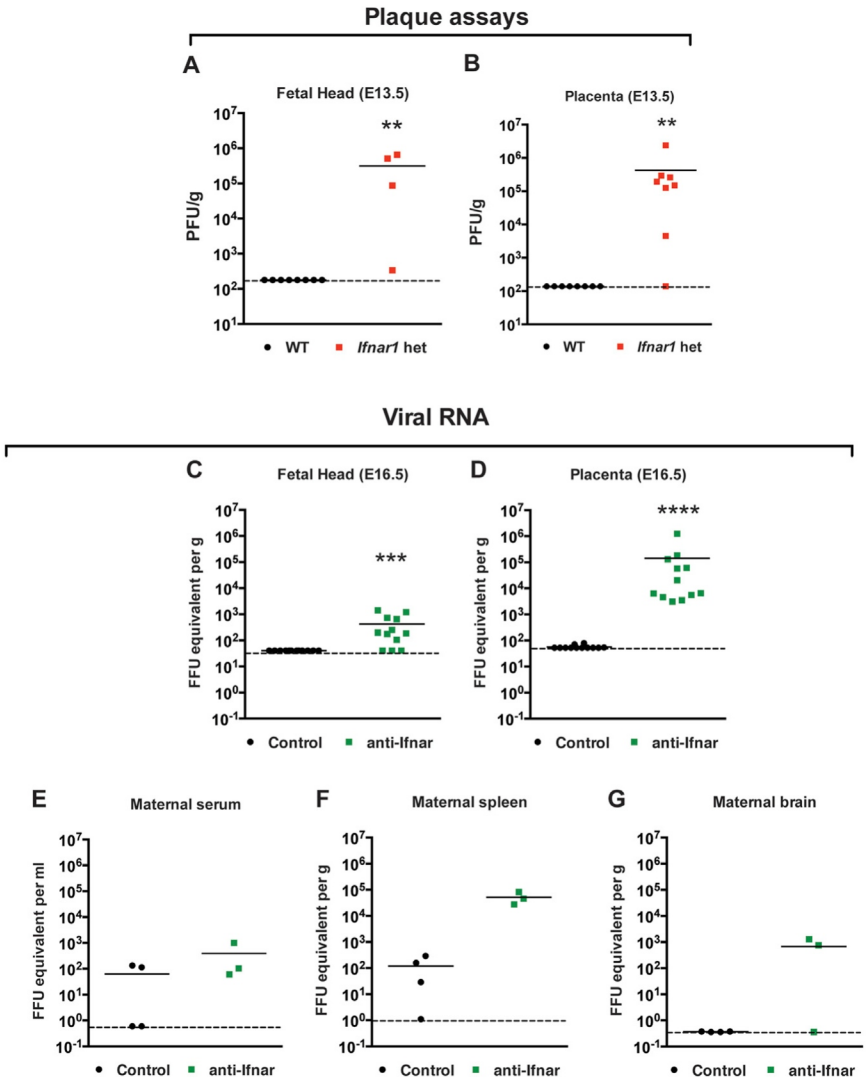


Figure S1. Viral Yield in the Placenta and Fetal Head, Related to Figure 1

Pregnant dams were infected with 10^3 FFU of ZIKV or via a subcutaneous route. A and B. Infectious virus detected by plaque assay in fetal head (A) and the placenta (B) on E13.5 after infection of *Ifnar1*$^{-/-}$ dams.

(C-G) Viral burden was measured by qRT-PCR assay from the fetal head (C), placenta (D), and in the indicated maternal tissues (E-G) on E16.5 after infection at E6.5 after dams were treated with anti-ifnar or control antibody. In this Figure, symbols represent individual fetuses or tissues pooled from 2 independent experiments with the exception of 4 intact *Ifnar1*$^{+/-}$ fetal heads that were carried by a single dam.

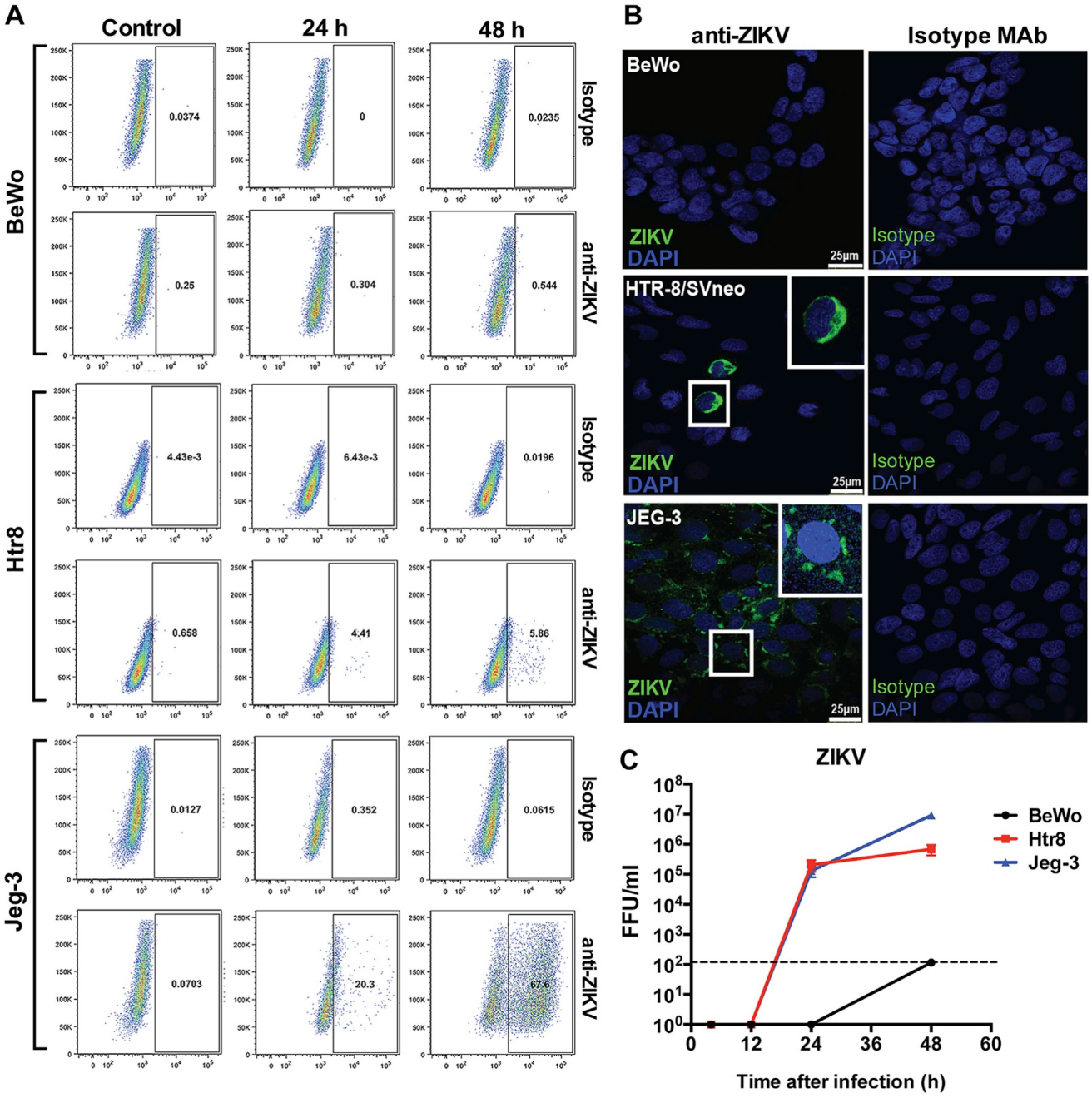


Figure S2. ZIKV Infects Human Trophoblast Cell Lines, Related to Figures 2 and 3

(A) Flow cytometry showing the efficiency of ZIKV infection in the indicated trophoblast cell lines. The indicated trophoblast cell lines were infected with ZIKV strain H/PF/2013 at MOI 0.1 for 2 hr, washed with PBS to remove the input virus, and collected at the indicated time points.

(B) Immunofluorescence microscopy of ZIKV infected trophoblasts at 48 hr post-infection using ZV-2, a ZIKV-specific mAb.

(C) Viral titer in the supernatants of ZIKV-infected trophoblasts at the indicated time points were assessed by infectious focus-forming assay on Vero cells. Results represent the mean ± SEM of two independent experiments.